

THE EVOLUTION OF A SHEARED REGION BETWEEN TWO CONTINUOUSLY STRATIFIED LAYERS

Hieu T. Pham*, Sutanu Sarkar†, Kyle A. Brucker‡
Department of Mechanical and Aerospace Engineering
University of California, San Diego
9500 Gilman Dr., La Jolla, CA, 92093, USA

ABSTRACT

Direct Numerical Simulations (DNS) are performed to investigate the behavior of a weakly stratified shear layer in the presence of a strongly stratified region beneath it. The stratification in the deep region measured by the Richardson number J_d has a value of 0.25. A traditional two-layer problem with the same bulk Richardson number is also simulated for comparison. Both coherent Kelvin-Helmholtz (KH) rollers and small-scale turbulence are observed during the evolution of the shear layer. The momentum thickness is smaller relative to the two-layer case although the evolution of the small scales are similar. In the J_d case, internal waves are excited, initially by KH rollers and later by small-scale turbulence. Waves generated by turbulence are relatively weaker with a broader range of frequencies. Integration of the turbulent kinetic energy budget in time and over the shear layer thickness shows that the energy flux can be up to 17% of the turbulent production, 33% of the turbulent dissipation rate and 75% of the buoyancy flux. These numbers illustrate the dynamical importance of internal waves. The mixing efficiency is found to be the same in both cases when the flow is in turbulent regime.

MOTIVATION

Stratified shear flow away from boundaries has been the subject of many studies, employing both experimental and numerical techniques. Nevertheless, there are only a handful that study the dynamics of a stratified shear layer in the presence of an external stratification where internal waves may be supported. Such a scenario can occur in the natural environment when the stratification extends continuously beyond the shear layer, and will be the focus of the current study. In the present study, we use direct numerical simulations (DNS) to investigate the properties of turbulence and mixing of an inhomogeneous stratified shear layer located between a weakly stratified upper layer and strongly stratified lower layer. We contrast the results with those observed in the typical mixing layer to illustrate differences and similarities in the following aspects: the evolution of the large-scale and small-scale structure in the shear layer, the evolution of the turbulent kinetic energy (TKE) budget insofar as the effects of internal wave excitation as well as the efficiency in turbulent mixing.

FORMULATION

Fig. 1 is a schematic of the simulated shear layer between two layers of fluid moving in opposite directions with a velocity difference ΔU and a vertical density stratification owing

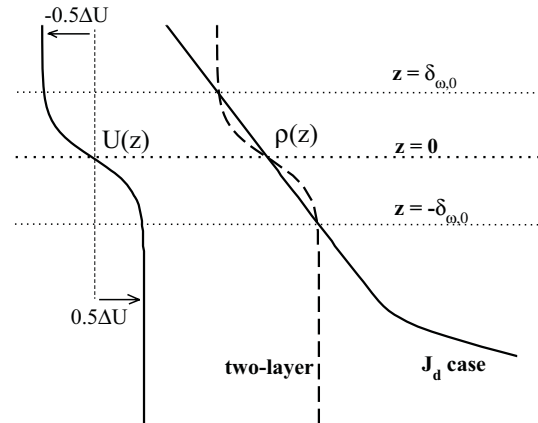


Figure 1: *Initial mean profiles.* Each case has a temporally evolving shear layer between two streams with velocity $-\Delta U/2$ and $\Delta U/2$, and initial vorticity thickness, $\delta_{\omega,0}$. The maximum shear is at $z = 0$. The two-layer density variation corresponds to a tangent-hyperbolic profile with $J(0) = 0.1$. The other density profile corresponds to a moderate linear stratification, $J_s = 0.05$, in the shear layer above a bottom region, $z < -2.5\delta_{\omega,0}$, with uniform stratification that takes the value $J_d = 0.25$. The initial value of bulk Richardson number, $Ri_{b,0} = 0.1$, is the same for both cases.

to a temperature variation. The flow evolves temporally with statistics that are homogenous in the streamwise (x) and spanwise (y) directions. The horizontal velocity varies continuously in the vertical cross stream direction (z) with a hyperbolic tangent profile,

$$\langle u \rangle = -\frac{\Delta U}{2} \tanh\left(\frac{2z}{\delta_{\omega,0}}\right),$$

where the initial vorticity thickness is defined by $\delta_{\omega,0} = \Delta U / (d\langle u \rangle / dz)_{max}$. The squared buoyancy frequency is defined by $N^2 = -(g/\rho_0) d\langle \rho \rangle / dz$ and a nondimensional measure of the stratification is the Richardson number, $J(z) = N(z)^2 \delta_{\omega,0}^2 / \Delta U^2$. Two types of density profile are considered. A two-layer density variation, corresponding to the classical Thorpe problem, is defined with a tangent-hyperbolic profile obtained by replacing ΔU in the mean velocity profile with the density change, $\Delta \rho$. The value of $\Delta \rho$ is chosen to set $J(z = 0) = 0.1$. The second type of density profile corresponds to a weakly stratified shear layer above a region of deep stratification. The fluid above and inside the shear layer region is linearly stratified with Richardson number $J_s = 0.05$. At depth $z = -2.5\delta_{\omega,0}$ the stratification changes to the value of the Richardson number specified in the deep region $J_d = 0.25$.

The initial shear layer vorticity thickness $\delta_{\omega,0}$, the density jump $\Delta \rho_0$ across twice the initial vorticity thickness, and the velocity difference ΔU are used for nondimen-

*h8pham@ucsd.edu

†sarkar@ucsd.edu

‡kbrucker@ucsd.edu

sionalization. We solve the Navier-Stokes equations under the Boussinesq approximation with the following nondimensional parameters: Reynolds number $Re = \Delta U \delta_{\omega,0} / \nu$, Prandtl number $Pr = \nu / \kappa$, and bulk Richardson number $Ri_{b,0} = (g \Delta \rho_0 \delta_{\omega,0}) / (\rho_0 \Delta U^2)$. Here, ν is the kinematic viscosity, and κ is the molecular diffusivity. Both simulations are run with $Re_0 = 1280$, $Pr = 1$ and $Ri_{b,0} = 0.1$.

The domain size is $51.6 \delta_{\omega,0} \times 17.2 \delta_{\omega,0} \times 96.57 \delta_{\omega,0}$ and the gridpoints in x, y, z directions are $384 \times 128 \times 512$, respectively. The grid is uniform in the streamwise and spanwise directions with the spacing of $0.134 \delta_{\omega,0}$. In the vertical direction the grid is uniform in the region $-7.5 < z < 2.5 \delta_{\omega,0}$ with the spacing of $0.0756 \delta_{\omega,0}$. Outside this region the grid is mildly stretched with a ratio of 2%. A second-order finite difference method on a staggered grid is used for spatial derivatives and a third-order Runge-Kutta method is used for time advancement. The flow is initialized with low amplitude velocity perturbations. Periodic boundary conditions are used in the x and y directions. Dirichlet boundary conditions are enforced for horizontal velocities and pressure while vertical velocity and density have Neumann conditions. A sponge region is employed at the top ($z > 15 \delta_{\omega,0}$) and the bottom ($z < -50 \delta_{\omega,0}$) boundaries to damp out internal waves propagating out of the domain. Evolution of the shear layer includes formation of KH rollers and their breakdown into small-scale three-dimensional turbulence. Simulations are continued until most of the fluctuations inside the shear layer is dissipated, roughly at $t_f = 250$ time units. Details of the numerical methods used in this study can be found in Basak & Sarkar (2006) and Brucker & Sarkar (2007).

EVOLUTION OF THE SHEAR LAYER

Shear instability, KH roller formation and transition to three-dimensional small-scale turbulence is typical for the evolution of the two layer case which has been studied extensively, e.g. Koop & Browand (1979); Smyth & Mowm (2000a,b). In the J_d case, the shear layer evolves in similar manner; nonetheless, the following differences are distinctive: inhibition of KH rollers pairing, early turbulence transition, internal wave excitation and significantly smaller shear layer thickness. In the following text, we elaborate on these observations with the visualization as well as the growth of the shear layer.

Fig. 2 gives the instantaneous density field in the vertical plane at $y = 8.5 \delta_{\omega,0}$ for the two simulated cases. The contrast in the evolution of the shear layer large-scale structures is eminent in Fig. 2(a) and (b). In the two-layer case, the KH rollers are larger and pair with one another while in the J_d case they quickly break down before pairing. The roller at $x = 5 \delta_{\omega,0}$ in Fig. 2(a) penetrates as deep as $z = -4 \delta_{\omega,0}$ while the two left-most rollers in Fig. 2(b) have already transitioned into turbulence. The pairing inhibition is due to the stronger stratification that the rollers experience at the base of the shear layer. In the J_d case, the rollers have to expend more kinetic energy to lift up the heavier fluid; both cases have the same initial amount of kinetic energy. As heavy fluid below is lifted above the shear layer into the region with lighter fluid, the lifted fluid carries significant amount of available potential energy and prefers to revert toward an energetically stable state leading to the early breaking of the KH rollers instead of growth through pairing. It should be noted that Fig. 2(a) corresponds to $t = 110$ when the large structure are still prominent while Fig. 2(b) corresponds to $t = 80$ when broadband turbulence

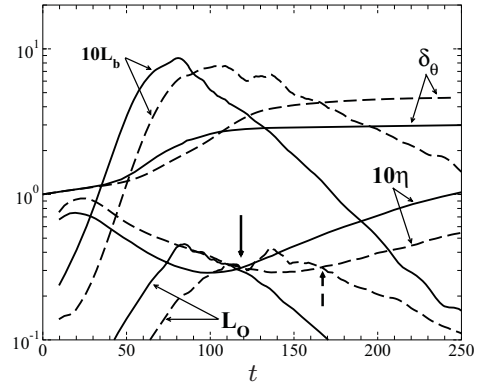


Figure 3: Evolution of the length scales: momentum thickness δ_θ , buoyancy scale L_b , Ozmidov scale L_O and Kolmogorov scale η . All scales are normalized with initial vorticity thickness $\delta_{\omega,0}$. Dashed lines indicate the two-layer case while solid lines denote the J_d case. The thick arrows indicate BIV transition.

is already present. Thus, in the J_d case, the inhibition of roller pairing causes an earlier transition to turbulence.

Instead of expending fluctuation energy to lift up heavier fluid, the shear layer in the J_d case radiates energy into the stratified interior via internal waves. Evidence of strong internal wave excitation is clearly shown by the coherent distortion of isopycnals in Fig. 2(b). The wave field is coherent over great depth and has a direct relation to the KH rollers: the wavelength of the internal waves is equal to the wavelength of the KH roller. The wave phase lines slant downward in the negative x -direction indicating that the wave group velocity is downward and upstream. Such a relationship resembles internal waves in flows over surface corrugations. The waves transport significant amount of energy away from the shear layer. The energetic consequences upon the evolution of the shear layer will be illustrated in the next section. Fig. 2(d) shows the shear layer in the J_d case at late time $t = 120$ when turbulence dominates. The isopycnals indicate small-scale turbulence can also excite internal waves. Waves excited by the turbulent shear layer are relatively weaker and span a broader spectrum than those excited by large-scale KH rollers. Compare Fig. 2(d) to (c), the turbulent shear layer in the J_d case is less energetic than that in the two-layer case. The turbulent shear layer in the latter case is thicker and contains finer scales indicating stronger mixing. The interface between the two fluids is thinner and much smoother in the J_d case.

To characterize the evolution of the shear layer, we track the growth of relevant length scales such as integral momentum thickness δ_θ , buoyancy scale L_b , Ozmidov scale L_O and Kolmogorov scale η . The evolutions of these length scales are shown in Fig. 3. It is noted that only momentum thickness gives the bulk description of the shear layer, the other length scales are computed only at center of the shear layer $z = 0$ in the following discussion.

The momentum thickness δ_θ , a typical measure of shear layer thickness, defined by

$$\delta_\theta = 4 \int_{z_l}^{z_u} \left(\frac{1}{4} - \frac{\langle u \rangle^2}{\Delta U^2} \right) dz. \quad (1)$$

Depths z_u and z_l are upper and lower bounds of the shear layer where the turbulence production is approximately zero but the Reynolds shear stress $\langle u'w' \rangle$ is not necessarily zero. The factor of 4 is used so that the initial momentum thickness is equal to the initial vorticity thickness $\delta_{\omega,0}$ used in

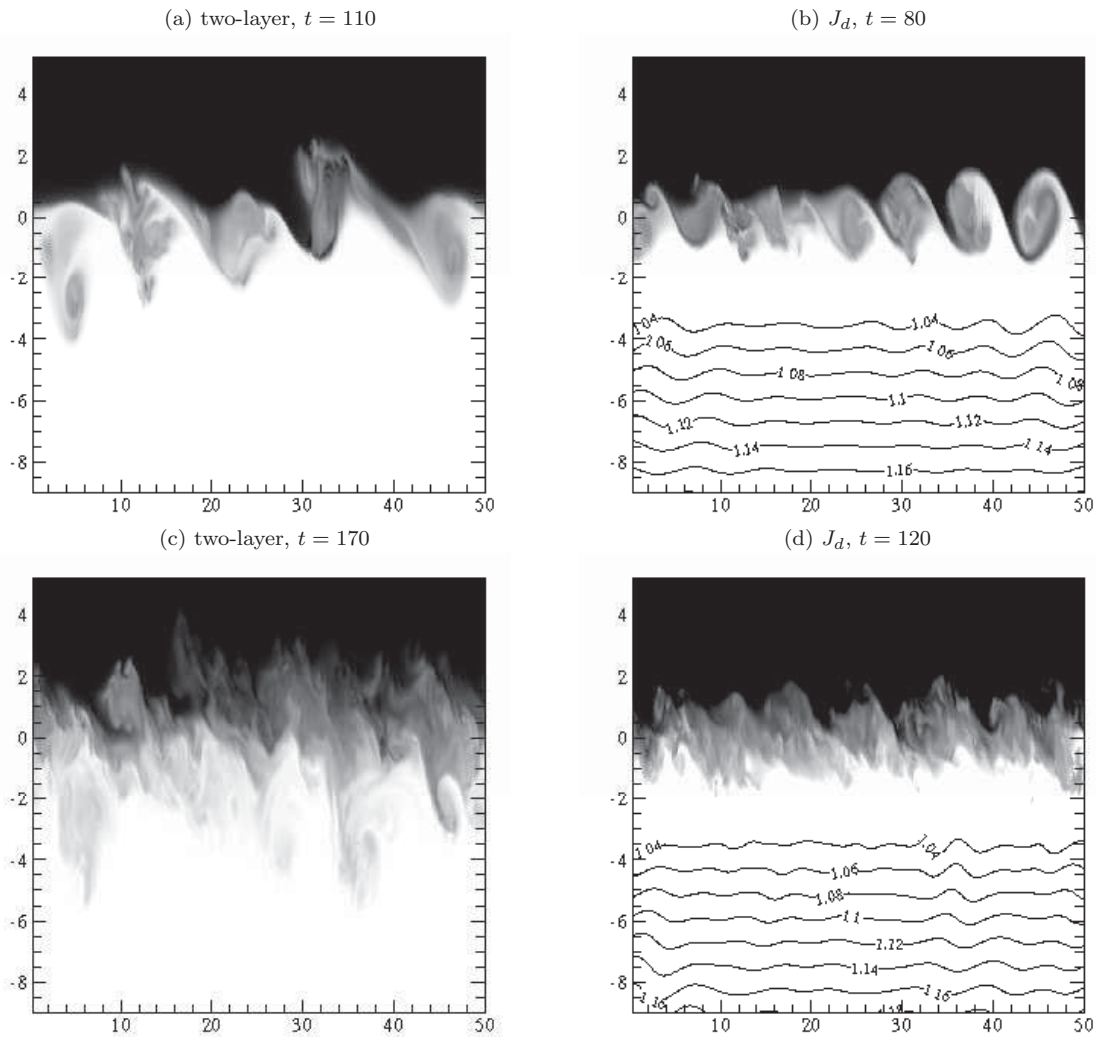


Figure 2: Density field in the vertical plane at $y = 8.5\delta_{\omega,0}$. The scale ranges from 99.5% (black) to 100.5% (white) ρ_0 . The isopycnals in (b) and (d) show the presence of internal waves in the J_d case while strong stirring is observed in the two-layer case.

nondimensionalization. Clearly, δ_θ grows less almost by half in the J_d case. Although the growth rate of the large-scale structure is the same in both cases, the growth period is short in the J_d case supporting the visual observation of pairing inhibition. At $t = 100$, δ_θ begins to become asymptotic in the J_d case while it continues to grow in the two-layer case.

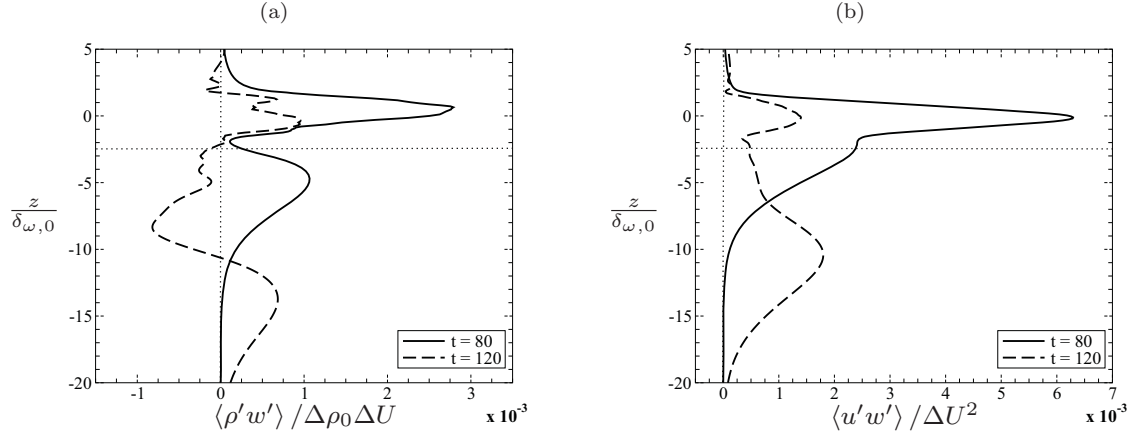
The evolution of the buoyancy length scale, defined by $L_b = w'_{rms}/N$, gives an estimate of the maximum distance a fluid parcel can be displaced in the vertical direction if all the kinetic energy is expended for such work. The growth of L_b in the two-layer case exhibits two local maxima at $t = 110$ corresponding to the KH rollers of largest size and at $t = 140$ corresponding to turbulent mixing. L_b in the J_d case peaks at earlier time and has only one maximum corresponding to the KH roller. After reaching the maximum value at $t = 80$, L_b decreases faster in the J_d case indicating that the energy-containing range of length scales in the turbulent shear layer is smaller than the corresponding range in the two-layer case. When L_b begins to decrease, δ_θ begins to become asymptotic indicating insignificant contribution of fluctuations to the shear layer thickness growth.

While L_b is related to buoyancy effects on the large-scale fluctuations, the Ozmidov scale L_O and Kolmogorov length scale η are pertinent to turbulent scales. The Ozmidov scale,

defined by $L_O = \sqrt{\epsilon/N^3}$, gives an estimate of the length scale below which the flow no longer feels the direct effect of buoyancy. The Kolmogorov scale, defined by $\eta = (\nu^3/\epsilon)^{1/4}$, is the scale at which energy is directly dissipated by molecular viscosity. When η reaches its smallest value, the shear layer is dominated by small-scale turbulence. Despite the different times at which they peak, the values of largest L_O and smallest η are the same in both cases indicating the background stratification in the deep region does not fundamentally alter the evolution of the small scales. The time at which L_O decreases to the value of 10η marks the buoyant-inertial-viscous (BIV) transition after which the inertial and buoyancy effects are damped out. As a result, the turbulence begins to decay due to viscosity. The thick arrows in Fig. 3 denote the BIV transition. The transition occurs early in the J_d case at $t = 120$ and later in the two-layer case at $t = 170$. The time period of strong turbulence indicated by $\eta > 10L_O$ is shorter in the J_d case approximately $80 < t < 120$ than in the two-layer case $110 < t < 170$.

TURBULENT KINETIC ENERGY

As discussed in the previous section, the presence of the external stratification affects the evolution of the length scales inside the shear layer. In this section, we use the TKE budget to illustrate the difference in the energetics,

Figure 4: J_d case. (a) Mass flux. (b) Momentum flux.

specifically the influence of internal waves that are allowed to propagate by the background stratification, external to the shear layer. It should be noted that TKE refers to the fluctuating energy due to both turbulence and waves. The TKE evolution equation is

$$\frac{dK}{dt} = P - \varepsilon + B - \frac{dT_3}{dz}. \quad (2)$$

Here, $K = 1/2 \langle u'_i u'_i \rangle$ is the TKE, $P = -\langle u'w' \rangle d\langle u \rangle / dz$ is the production rate, $B = -(g/\rho_0) \langle \rho'w' \rangle$ is the buoyancy flux, and $\varepsilon = (2/Re_0) \langle s'_{ij} s'_{ij} \rangle$ is the dissipation rate. s'_{ij} is the fluctuating strain rate and the bracket denotes horizontal plane average. The transport term dT_3/dz is defined with

$$T_3 = \frac{1}{2} [\langle w'u'u' \rangle + \langle w'v'v' \rangle + \langle w'w'w' \rangle] - \frac{2}{Re_0} [\langle u's'_{31} \rangle + \langle v's'_{32} \rangle + \langle w's'_{33} \rangle] + \frac{\langle p'w' \rangle}{\rho_0}.$$

The terms in the first bracket represent turbulent transport, those in the second bracket represent viscous diffusion while the $\langle p'w' \rangle / \rho_0$ term represents the pressure transport, an indication of energy flux by internal waves.

Before discussing the TKE budget, it is beneficial to first examine the wave fluxes in the J_d case. Fig. 4 shows the profiles of mass flux $\langle \rho'w' \rangle$ in (a) and momentum flux $\langle u'w' \rangle$ in (b) at $t = 80$ and 120 marking, respectively, the beginning and the end of the period of strong turbulence. At $t = 80$, there is an upward mass flux in the region $-10 < z < -2.5\delta_{\omega,0}$. This is followed by a downward flux in that region at $t = 120$. Integration in time of the mass flux at $z = -5\delta_{\omega,0}$ indicates that there is almost no net transport, agreeing with linear theory. Nonetheless, it should be noted that there is a diffusion of mass due to the stratification difference between the region above and below the shear layer. Mass is accumulated in the transition layer at $z = -2.5\delta_{\omega,0}$ where the upper and lower stratification merges. The accumulation is steady throughout the simulation. Although the waves do not transport mass, they extract significant amount of momentum from the shear layer as shown in Fig. 4(b). The momentum flux $\langle u'w' \rangle$ of the KH-excited waves at $t = 80$ at $z = -2.5\delta_{\omega,0}$ is as large as 35% of the Reynolds stress extracted from the mean shear at $z = 0$. Waves excited by small-scale turbulence at $t = 120$ transport significantly less momentum.

Since there are two types of internal waves: KH-excited and turbulence-excited, we present the TKE budgets at $t = 80$ and 120 to illustrate the effect of each type of wave upon the shear layer energetics. Fig. 5(a) shows the budget at $t =$

80 when the flow is dominated by the large-scale KH rollers. The production dominates over other terms resulting in an accumulation of TKE in the shear layer. Energy transport due to waves is evident in buoyancy flux B , transport dT_3/dz and transient term dK/dt . Integrating the budget from the top boundary of the domain down to $z = -2.5\delta_{\omega,0}$ yields the relative efficiency of wave transport. Fig. 5(b) shows the profiles of wave transport, $IW = \langle p'w' \rangle / \rho_0$, normalized by other terms in the integrated budget. At $z = -2.5\delta_{\omega,0}$, turbulent transport is insignificant and, therefore, only the wave transport is plotted. Clearly, a large amount of energy is extracted from the shear layer by the KH-excited waves. The extraction can be up to 25% of the production and 100% of the dissipation. The internal wave flux is 160% of the buoyancy flux; in other words, at this time the shear layer loses more energy to waves than the amount expended in local stirring of the density field.

At $t = 120$, the dissipation dominates the shear layer as shown in Fig. 6(a). Compare the waves excited by large structure (below $z = -5\delta_{\omega,0}$) and those excited by small-scale turbulence (in the region $-2.5 < z < -5\delta_{\omega,0}$), the latter are less energetic. The transport efficiency discussed above is shown in Fig. 6(b). Relative to the integrated production and dissipation, the energy lost to turbulence-excited waves is insignificant as shown by the small values at $z = -2.5\delta_{\omega,0}$. Nevertheless, the wave energy flux at $z = -2.5\delta_{\omega,0}$ is about 50% of the integrated buoyancy flux. The efficiency shown here agrees well with the values reported in the study of Taylor & Sarkar (2007) where they investigate the internal waves generated by wall turbulence. Also clear in Fig. 6(a) is that the KH-excited waves have low dissipation and exhibit energy equipartition. Of the amount of energy transported out of the shear layer by waves dT_3/dz , half goes to the wave kinetic energy dK/dt and half is expended to raise the fluctuating potential energy B . Such equipartition further substantiates the linear behavior of the KH-excited waves.

We now characterize the energetics of the fluctuations during the entire evolution rather than at the two specific times of Fig. 5 and 6. Fig. 7 shows the time evolution of terms in the integrated TKE budget in the J_d case. The spatial integration is from z_{max} down to depth $z = -5\delta_{\omega,0}$. As the vortices roll up, a significant amount of energy is extracted from mean shear by fluctuations through the turbulent production, some of which is used to increase turbulent kinetic energy. The buoyancy flux also reaches its maximum value early since larger eddies have the capability to lift up heavy fluid. The peak dissipation rate occurs at later time when the flow turns turbulent. The wave pressure transport term IW is significant and occurs at a time between the

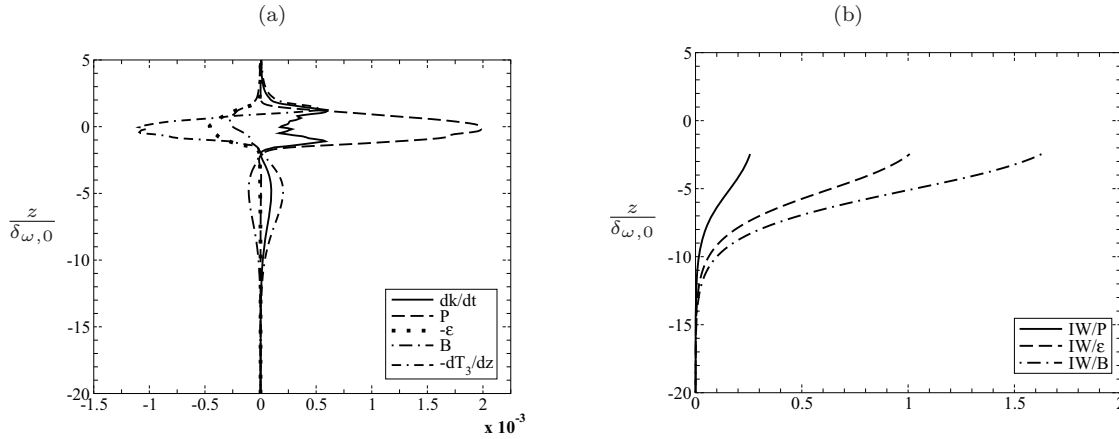


Figure 5: J_d case. (a) TKE budget at $t = 80$. (b) Wave transport efficiency, the absolute ratio of the wave transport, $IW = \langle p'w' \rangle / \rho_0$, to the terms shown in (a) after being spatially integrated. The integration is from z_{max} down to $z = -2.5\delta_{\omega,0}$.

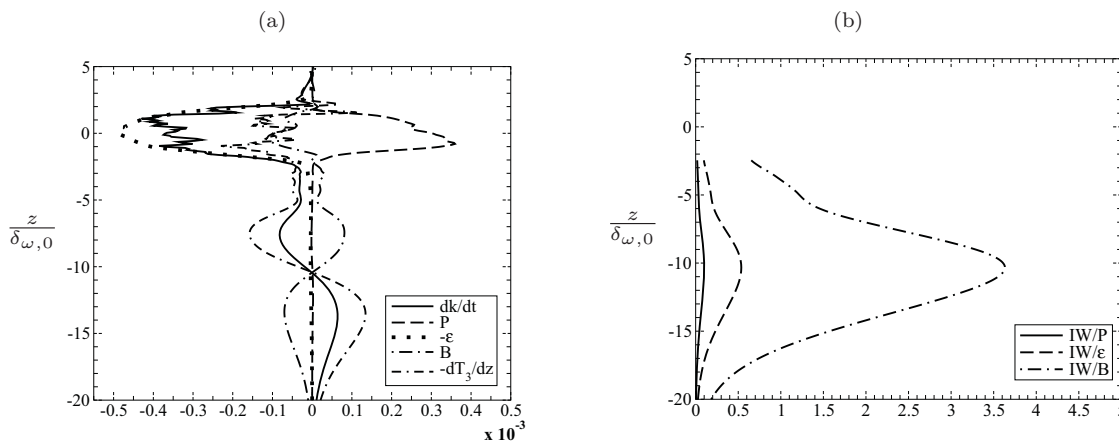


Figure 6: J_d case. (a) TKE budget at $t = 120$. (b) Wave transport efficiency. See caption in Fig. 5.

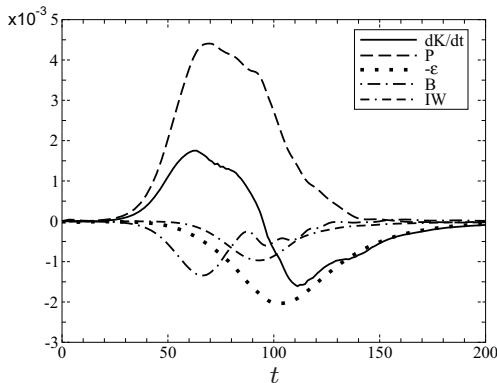


Figure 7: Integrated TKE budget in the J_d case. The production, dissipation and buoyancy flux are integrated from z_{max} to $z = -5\delta_{\omega,0}$, depth at which $IW = \langle p'w' \rangle / \rho_0$ is measured.

occurrence of peak production and peak dissipation.

An overall quantification of the efficiency of internal wave flux is obtained by integrating the profiles in Fig. 7 from time $t = 0$ to late time t_f when the turbulent kinetic energy inside the shear layer vanishes. This procedure is convenient since the temporal peak values of the various terms in the TKE balance occur at different times. The partition of the extracted energy into the various sinks of the TKE balance is as follows: 53% of the production is dissipated, 23% is used for stirring the density field, and 17% is transported away by internal waves. In the two-layer case, 65% of the extracted energy is dissipated and 28% is used for mixing. The difference between the two cases shows that internal

waves supported by the external stratification substantially alters the turbulence energetics inside the shear layer.

MIXING EFFICIENCY

In previous section, we have illustrated that buoyancy flux, i.e. TKE used for stirring, is less in the J_d case. In this section we focus the wave role in mixing. We first examine the evolution of the density variance which is governed by

$$\frac{d}{dt} \langle \rho'^2 \rangle = P_\rho - \chi_\rho - \frac{dT_\rho}{dz}, \quad (3)$$

where $P_\rho = -2 \langle \rho'w' \rangle d \langle \rho \rangle / dz$ is the production, and $\chi_\rho = (2/PrRe_0) \langle (\partial \rho' / \partial x_i)^2 \rangle$ is the thermal dissipation. The transport term is

$$\frac{dT_\rho}{dz} = \frac{\partial \langle \rho'^2 w' \rangle}{\partial z} - \frac{1}{PrRe_0} \frac{\partial^2 \langle \rho'^2 \rangle}{\partial z^2}.$$

The terms in the density variance budget for the two-layer case are shown in Fig. 8(a) at $t = 110$ and ones for the J_d case are shown in Fig. 8(b) at $t = 80$. These are the times at which the maximum buoyancy scale L_b occurs. In the two-layer case, the profiles are restricted in the shear layer where the dissipation can be as large as the production. The dissipation in the shear layer is slightly higher in the J_d case. The production is not symmetric across the shear center $z = 0$ as in the two-layer case due to the asymmetry in the background stratification. The production in the J_d case is larger in the upper-half of the shear layer where there is no wave flux. In the region below the shear layer, nearly all the

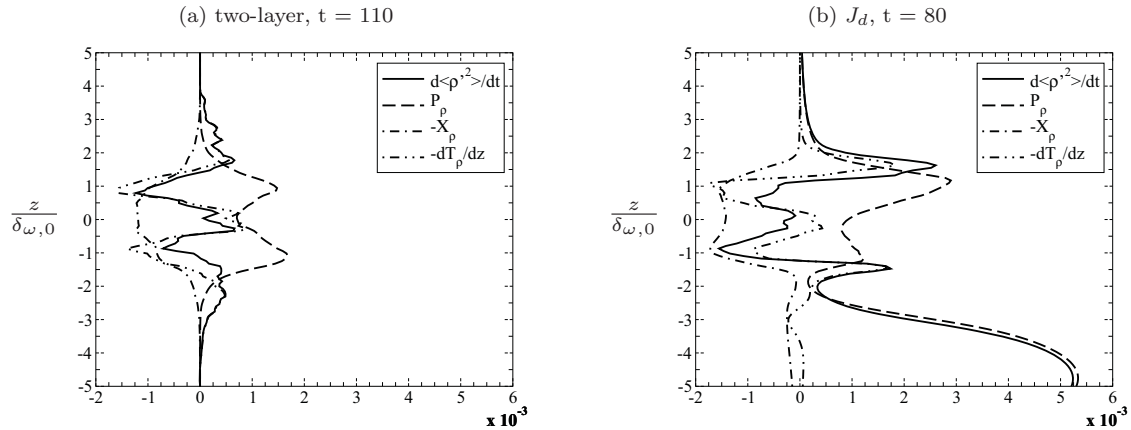


Figure 8: Budget of density variance $\langle \rho'^2 \rangle$ in the two-layer case (a) and J_d case (b).

transient gain is due to the production. The internal wave is nearly non-dissipative.

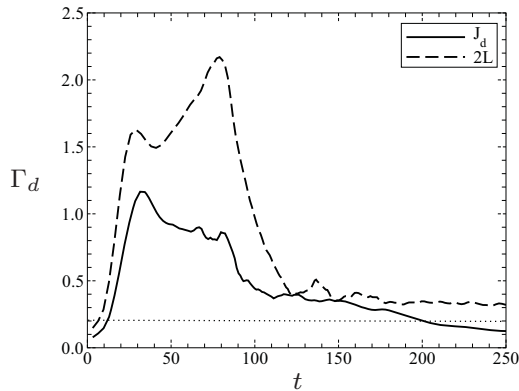


Figure 9: Evolution of mixing efficiency Γ_d measured at the shear center $z = 0$ in both cases. Horizontal dotted line indicates frequently used value $\Gamma_d = 0.2$.

To evaluate the mixing efficiency, we examine the quantity $\Gamma_d = \epsilon_\rho / \epsilon$ which can be measured directly in the ocean from temperature gradient and velocity shear data. Here, ϵ_ρ is defined by

$$\epsilon_\rho = \frac{1}{2} \frac{g}{\rho_0 |d\langle \rho \rangle / dz|} \chi_\rho,$$

where ϵ_ρ signifies irreversible loss of turbulent potential energy to the background density field. Fig. 9 shows the time evolution of Γ_d measured at the shear center in both cases. The mixing efficiency is large when large-scale structure is present in the shear layer. In the presence of the KH rollers, the two-layer case has larger Γ_d due to larger ϵ_ρ recalling the viscous dissipation ϵ is similar in both cases as shown in the evolution of Kolmogorov scale η in Fig. 3. Although $\Gamma = \Gamma_d = 0.2$ is often employed, the value can depend on the type of flow, the age of the flow in non-stationary examples, as well as other parameters such as Reynolds number, Richardson number, and Prandtl number. Here, the value is about 0.4 in both cases when the flow is highly turbulent. Γ_d persists at the asymptotic value for a long time in the two-layer case while it decreases in the J_d case.

CONCLUSIONS

The direct numerical simulations conducted here show that the presence of an external stratified region substantially changes the evolution of a stratified shear layer when compared to the typical situation of shear between two layers, each with constant density that differs. The J_d case has significantly smaller momentum thickness δ_θ with respect to

the two-layer situation although the peak values of buoyancy scale, Ozmidov scale and Kolmogorov scale are the same in both cases. The peak values of these scales as well as the BIV transition occur early such that the flow becomes turbulent at earlier time in the J_d case. The shear layer in the J_d case excites strong internal waves. Internal waves, observed here to propagate in the bottom interior region, do not transport mass away or into the shear layer, consistent with linear wave theory, but are shown to constitute a significant pathway for energy transfer into the interior. Integration of the kinetic energy budget over the simulated time shows that the internal waves are important to the energetics of the shear layer. The waves can take up to 17% of the energy extracted from the mean shear. Although significant energy is lost due to waves, the mixing efficiency during the turbulent period is the same for both the J_d case and the two-layer case.

REFERENCES

- BASAK, S. & SARKAR, S. 2006 Dynamics of a stratified shear layer with horizontal shear. *J. Fluid Mech.* **568**, 19–54.
- BRUCKER, K. & SARKAR, S. 2007 Evolution of an initially turbulent stratified shear layer. *Phys. Fluids* **19**, 101105.
- KOOP, C. G. & BROWAND, F. K. 1979 Instability and turbulence in a stratified fluid with shear. *J. Fluid Mech.* **93**, 135–159.
- SMYTH, W. D. & MOUM, J. N. 2000a Anisotropy of turbulence in stably stratified mixing layers. *Phys. Fluids* **12** (6), 1343–1362.
- SMYTH, W. D. & MOUM, J. N. 2000b Length scales of turbulence in stably stratified mixing layers. *Phys. Fluids* **12** (6), 1327–1342.
- TAYLOR, J. & SARKAR, S. 2007 Internal gravity waves generated by a turbulent bottom ekman layer. *J. Fluid Mech.* **590**, 331–354.